FULL-LENGTH ORIGINAL RESEARCH

The antiepileptic medications carbamazepine and phenytoin inhibit native sodium currents in murine osteoblasts

*†‡§¶Sandra J. Petty, †Carol J. Milligan, *Marian Todaro, †Kay L. Richards, #Pamuditha K. Kularathna, #Charles N. Pagel, *‡¶Chris R. French, **Elisa L. Hill-Yardin, *‡¶Terence J. O'Brien, ¶††John D. Wark, #Eleanor J. Mackie, and †Steven Petrou

Epilepsia, **(*):1–8, 2016
doi: 10.1111/epi.13474

Dr. Sandra Petty is a clinical and academic neurologist at The University of Melbourne

Dr. Carol Milligan is a senior research officer at the Florey Institute of Neuroscience and Mental Health in Melbourne

Summary

Objective: **Fracture risk is a serious comorbidity in epilepsy and may relate to the use of antiepileptic drugs (AEDs). Many AEDs inhibit ion channel function, and the expression of these channels in osteoblasts raises the question of whether altered bone signaling increases bone fragility. We aimed to confirm the expression of voltage-gated sodium (Na_V) channels in mouse osteoblasts, and to investigate the action of carbamazepine and phenytoin on Na_V channels.**

Methods: **Immunocytochemistry was performed on primary calvarial osteoblasts extracted from neonatal C57BL/6J mice and additional RNA sequencing (RNASeq) was included to confirm expression of Na_V. Whole-cell patch-clamp recordings were made to identify the native currents expressed and to assess the actions of carbamazepine (50 μM) or phenytoin (50 μM).**

Results: **Na_V expression was demonstrated with immunocytochemistry, RNA sequencing, and functionally, with demonstration of robust tetrodotoxin-sensitive and voltage-activated inward currents. Application of carbamazepine or phenytoin resulted in significant inhibition of current amplitude for carbamazepine (31.6 ± 5.9%, $n = 9$; $p < 0.001$), and for phenytoin (35.5 ± 6.9%, $n = 7$; $p < 0.001$).**

Significance: **Mouse osteoblasts express Na_V, and native Na_V currents are blocked by carbamazepine and phenytoin, supporting our hypothesis that AEDs can directly influence osteoblast function and potentially affect bone strength.**

KEY WORDS: **Epilepsy, Bone health, Osteoblast, Voltage-gated sodium channel, Electrophysiology.**

Accepted June 22, 2016.

*The Department of Medicine, Melbourne Brain Centre at The Royal Melbourne Hospital, The University of Melbourne, Parkville, Victoria, Australia; †The Florey Institute of Neuroscience and Mental Health, Parkville, Victoria, Australia; ‡Department of Neurology, The Royal Melbourne Hospital, Parkville, Victoria, Australia; §Academic Centre, Ormond College, Parkville, Victoria, Australia; ¶Department of Medicine, The Royal Melbourne Hospital, The University of Melbourne, Parkville, Victoria, Australia.; #Faculty of Veterinary and Agricultural Sciences, The University of Melbourne, Parkville, Victoria, Australia; **Department of Physiology, University of Melbourne, Parkville, Victoria, Australia; and ††Bone and Mineral Medicine, The Royal Melbourne Hospital, Parkville, Victoria, Australia

Address correspondence to Sandra Petty, Department of Medicine, The University of Melbourne, 1st Floor, Kenneth Myer Building, Parkville, Vic. 3052, Australia. E-mail: pettys@unimelb.edu.au

S. J. Petty and C. J. Milligan equal first authorship.

Key Points

- Immunocytochemistry and automated electrophysiology showed functional expression of voltage-gated sodium currents in mouse primary osteoblasts
- Carbamazepine and phenytoin resulted in significant inhibition of sodium current amplitude
- The inhibition of sodium currents in osteoblasts by AEDs is a potential mechanism for altered bone strength in epilepsy

Patients with epilepsy have at least doubled fracture risk.[1] A proportion of patients with epilepsy, particularly those who have taken long-term antiepileptic drug (AED) therapy, have reduced bone density.[2–4] Causes of these associations are not fully understood,[1,5] particularly whether there are direct bone side effects of AEDs. Approximately 1% of the population requires AED treatment for epilepsy, often for prolonged duration,[6] with important treatment benefits, but also a risk of long-term adverse health effects.[2,7,8] More widespread use of AEDs for newer indications including migraine, chronic pain, and bipolar affective disorder, increases the imperative to determine whether AEDs increase fracture risk and, if so, by what mechanism(s). A more complete understanding of the mechanism for impaired bone health in epilepsy should facilitate the development of safer medications.

Initially, effects of AEDs on vitamin D metabolism were proposed as the primary mechanism for bone disease[9]; however, use of noninducer AEDs (which do not impact vitamin D metabolism) is also associated with bone disease.[10,11] Furthermore, there is a poor relationship between bone fracture risk and circulating vitamin D metabolite levels.[3] AEDs have multiple mechanisms of action; however, they all influence neuronal cellular signaling to exert their effects. In a similar fashion, AEDs may affect bone cell signaling, which may underlie a decrease in bone strength. Ion channels are common targets of many AEDs, and both osteoblasts and osteocytes express ion channels, including some voltage-gated ion channels.[12–14] Ion channels have been implicated in transducing bone stress and strain,[15–17] critical for modeling and remodeling. Although osteocytes are often considered the primary mechanosensing cells in bone, osteoblasts also are capable of responding to mechanical stress.[18] Osteoblasts possess multiple ion channels, including hyperpolarization and osmolarity-sensitive channels,[19] and voltage-gated sodium (Na_V) channels.[20] Another study observed rapid effects of vitamin D3 on voltage-gated L-type Ca2+ channel and mechanosensitive chloride channels in the osteoblastic ROS 17/2.8 cell line and primary osteoblasts, and proposed that this mechanism may contribute to the ability of vitamin D to promote osteoblast secretory function; Na_V channels were not included in that study.[21] Electric coupling between both rat and guinea pig osteoblast-like cells was reported to be inhibited up to 59% by carbamazepine (CBZ) and phenytoin (PHT), and the membrane potential depolarized by approximately 40–45% following use of CBZ; however, specific effects of AEDs upon Na_V channels were not assessed in that study. Na_V channels have a long-established role in electrogenesis in neurons,[22] and they are also expressed in "nonexcitable" cells, with a range of effector functions, including attenuating cellular motility and migration, and driving reverse calcium importing in Na/Ca exchange.[23] Traditionally, osteoblasts are considered "nonexcitable" cells[23]; however, there are ion channels present in osteoblasts that allow action potentials to be fired.[20] The role of Na_V channels in osteoblasts and effects of AEDs such as CBZ and PHT on Na_V channels in osteoblasts require investigation. We chose to initially investigate the AEDs CBZ and PHT, as they have been associated with reduced bone mineral density (BMD)[3,7] and fractures.[24–26] In this study, we investigated CBZ and PHT effects on Na_V channels using whole-cell patch-clamp recording in mouse osteoblasts to evaluate a direct effect of these AEDs on osteoblasts. Better identification of the mechanisms underlying increased fracture rate and changes in bone quality seen in association with epilepsy and its treatment will allow for improving the targeting of fracture prevention strategies in patients with epilepsy.

Materials and Methods

Calvarial digests and cell culture

Primary osteoblasts were isolated from calvariae of C57BL/6J neonatal mice utilizing a previously published sequential collagenase digest protocol[27] with minor modifications. Briefly, calvariae were incubated in fresh digestion buffer containing collagenase type 1 (140 Units/ml) (Worthington Biochemical Corporation, Lakewood NJ, U.S.A.), 0.05% (w/v) trypsin (Invitrogen, Carlsbad, CA, U.S.A.), and 2.5 mM $CaCl_2$ in Dulbecco's phosphate-buffered saline (PBS) at 37°C six times for 20 min. Primary calvarial mouse osteoblasts were then maintained in alpha Minimum Essential Media (αMEM) supplemented with 10% (v/v) fetal bovine serum (FBS) and gentamicin (50 μg/ml) (Gibco Life Technologies, Grand Island, NY, U.S.A.) in culture flasks (BD Falcon, San Diego, CA, U.S.A.). Medium was changed every 3–4 days and cells were maintained as subconfluent cultures in a humidified incubator with 5% CO_2 in air at 37°C. Samples of the cultured cells were stained for alkaline phosphatase (Sigma-Aldrich, St Louis, MO, U.S.A.) to confirm osteoblastic characteristics, and cells from digests that were positive for alkaline phosphatase were included in the Patchliner (Nanion Technologies, Munich, Germany) experiments.

Ethics approvals were obtained from the Howard Florey Institute Animal Ethics Committee (project number 13-028-UM), and all experiments were conducted in accordance

with the Australian National Health and Medical Research Council (NHMRC) guidelines on the ethical use of animals in scientific research.[28]

RNASeq analysis

First-passage cells were grown until subconfluent in Dulbecco's Modified Eagle Medium (DMEM) containing L-glutamine (2 mM) and 10% FBS, and then cultured in Biological Research Faculty and Facility-Human Prostate Cell Serum Free medium (BRFF-HPC1) medium (Athena Enzyme Systems, Baltimore, MD, U.S.A.) containing 10% FBS for 48 h. Total RNA was extracted from three individual osteoblast isolates. Libraries were prepared from total RNA (5 μg) using the TruSeq RNA v2 sample preparation protocol (Illumina, San Diego, CA, U.S.A.); 100 base pair paired-end sequencing was conducted using the HiSeq 2000 platform (Illumina) at the Australian Genomics Research Facility (Parkville, Australia), according to the manufacturer's instructions. After filtering and trimming, reads were mapped to the mouse reference genome assembly GRCm38/mm10 using the program TopHat,[29] prior to transcripts being assembled from the aligned reads, using the program Cufflinks.[30] Results were expressed as FPKM (fragments per kilobase of exon per million fragments mapped), and a threshold of 0.3 was applied to FPKM as per previously described heuristic techniques[31]; 95% confidence intervals for FPKM were calculated.

Cell staining and microscopy

Primary calvarial osteoblast culture samples were stained for alkaline phosphatase to confirm osteoblastic characteristics using a kit (Sigma-Aldrich, Cat# 86C-1KT). Immunocytochemistry was performed using rabbit anti-rat Na_V (Panα) (1:500; Cat # S6936) and Alexa-488–conjugated goat anti-rabbit Ig (1:300; Molecular Probes, Cat# A11034); nuclei were counterstained using 4′,6-diamidino-2-phenylindole (DAPI) (0.33 μg/ml, Cat # D9542; Sigma-Aldrich). Fluorescent images were acquired using an Olympus FV1000 confocal microscope with an Olympus 60× oil objective (NA 1.35).

Electrophysiologic recordings

Electrical recordings were conducted using the Patchliner in the whole-cell configuration. Before recordings, cells were detached from culture flasks with Accutase Cell Detachment Solution (Innovative Cell Technologies Inc., San Diego, CA, U.S.A.) and resuspended at a density of 1×10^6 to 5×10^7/ml in 50% αMEM (without FBS) and 50% external recording solution v/v. The external recording solution comprised (mmol/L): 140 NaCl, 4 KCl, 1 $MgCl_2$, 2 $CaCl_2$, 5 D-glucose, 10 HEPES, and 10 tetraethylammonium (TEA) (pH 7.4 with NaOH). The osmolarity of this solution was 298 mOsm. The internal recording solution comprised (mmol/L): 50 CsCl, 10 NaCl, 60 CsF, 2 $MgCl_2$, 20 ethylene glycol tetraacetic acid (EGTA), 10 4-(2-hydroxyethyl)-1-piperazineethanesulfonic acid) (HEPES), 3 Mg^{2+}-adenosine 5′-triphosphate, and 10 tetraethylammonium (TEA) (pH 7.2 with CsOH), and the osmolarity of this solution was 285 mOsm. Solutions were filtered using a 0.2 μm membrane filter (Minisart; Sartorius Stedim Biotech, Goettingen, Germany). Cells were kept in suspension by gentle automatic pipetting. Medium single-hole planar NPC®-16 chips (Nanion Technologies) with an average resistance of ~2.5 MΩ were used. Pipette and whole cell capacitance were fully compensated and the series resistance compensation was set to 50%. Recordings were acquired at 50 kHz with the low-pass filter set to 3 kHz in PATCHMASTER (HEKA Instruments Inc., Bellmore, NY, U.S.A.) and performed at 27°C. Offline analysis was performed using Microsoft Excel and GraphPad Prism 6 (Molecular Devices). Data are shown as means ± standard error of the mean (SEM). Leak subtraction was performed in software before the currents were normalized. Statistical analysis was performed using Student's *t*-test, and differences were considered significant when $p < 0.05$.

Pulse protocols

The voltage dependence of activation was studied by measuring the normalized peak currents during 100 msec depolarizations from −120 mV to +30 mV in 5 mV increments. The resulting I–V curve was fit to the equation $I = [1 + \exp(-0.03937.z.(V - V_{1/2})] - 1.g.(V - V_r)$ (I, current amplitude; z, apparent gating charge; V test potential; $V_{1/2}$, half maximal voltage; g, factor related to the maximum number of open channels; and V_r, reversal potential). Conductance was determined using $G = I/(V - V_r)$. To study the steady-state fast inactivation, cells were held at conditioning pre-pulse potentials ranging from −120 mV to +30 mV in 5 mV increments from a holding potential of −120 mV and a test pulse at 0 mV for 20 msec. The peak current amplitudes during the subsequent test pulses were normalized to the peak current amplitude during the first test pulse and plotted against the potential of the conditioning pulse. Recovery from fast inactivation was studied by prepulsing the cells to 0 mV from a holding potential of −120 mV for 30 msec to fully inactivate channels. The voltage was then returned to the holding potential of −120 mV for variable intervals (every 3 msec from 0 to 39 msec). Finally, the voltage was stepped to 0 mV for 30 msec to test channel availability. The peak current amplitude during the test potentials was plotted as fractional recovery against the recovery period by normalizing to the maximum current during the conditioning potentials. The recovery currents were plotted against delta time.

To examine the effects of AEDs, two voltage protocols were used. In the first, the cells were held at −60 mV and 20 msec test depolarizations were applied in 10 mV increments, from −80 mV to +60 mV. The cells were then exposed to vehicle control dimethyl sulfoxide (DMSO), followed by 50 μM CBZ and then 10 μM tetrodotoxin TTX

in the continued presence of 50 μM CBZ and the voltage protocol utilized for each variable. In the second set of experiments, cells were held at −60 mV and 20 msec duration test depolarizations applied every 2 s in the presence of vehicle. Data were acquired for 3–5 min to establish a stable control baseline current, during which time vehicle was continuously applied. On establishment of a stable current, CBZ (50 μM) or PHT (50 μM) was applied to the cells for 5 min. Following 3–5 min washout of AED, 10 μM TTX was applied for 2 min. Peak currents for individual cells were averaged over 30 s periods directly before application of AED, following establishment of block in the presence of AED and following establishment of block by TTX.

Results

We identified the presence of functional Na_V channels in primary mouse osteoblasts using RNASeq, immunohistochemistry, and patch-clamp electrophysiologic techniques. RNASeq analysis was used to determine whether Na_V channels are expressed by primary mouse osteoblast cultures. Utilizing a threshold of 0.3 FPKM, a number of genes encoding Na_V channels (including α and β subunits) were found to be expressed (Table 1). Expression of the genes *Scn2a1* (Na_V 1.2), *Scn3a* (Na_V 1.3), *Scn7a* (also referred to as *Scn6a*, NaG, Na_X, $Na_{Vi}2.1$, $Na_V2.1$, or $Na_V2.2$), *Scn1b* ($Na_V\beta1$), and *Scn3b* ($Na_V\beta3$) was revealed using this

Table 1. RNAseq results for genes expressed encoding Na_V channels (including alpha and beta subunits): FPKM > 0.3, and 95% confidence intervals

Gene symbol	Gene name; synonym	FPKM	95% CI low	95% CI high
Scn2a1	Sodium channel, voltage gated, type II alpha subunit; $Na_V1.2$	1.4821	0.9256	2.0404
Scn3a	Sodium channel, voltage gated, type III alpha subunit; $Na_V1.3$	0.5222	0.2786	0.7631
Scn7a	Sodium channel, voltage gated, type VII alpha subunit; $Na_{Vi}2.1$	3.6029	2.4555	4.7530
Scn1b	Sodium channel, voltage gated, type I beta subunit	34.8005	22.9675	45.8203
Scn3b	Sodium channel, voltage gated, type III beta subunit	2.1051	1.2063	3.0036

FPKM, fragments per kilobase of exon per million fragments mapped; CI, confidence interval.

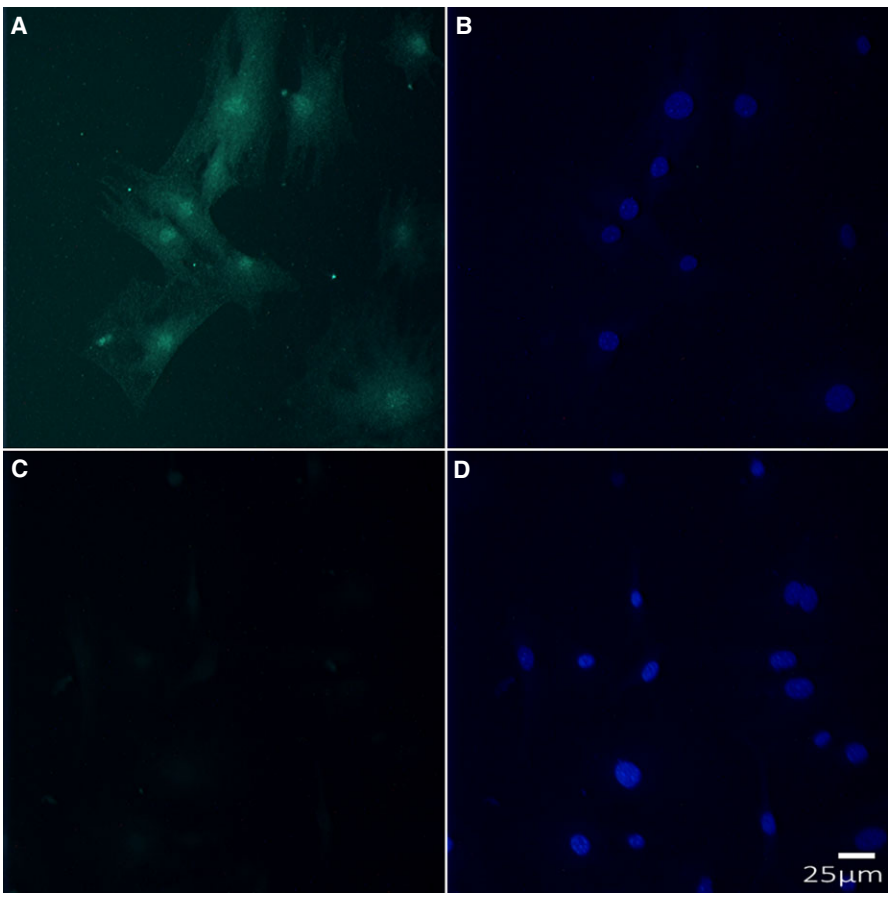

Figure 1.
Immunocytochemistry staining of cells from mouse calvarial osteoblast cultures with Na_V (Pan-α) antibody and DAPI nuclear counterstaining. (**A**) Na_V (Pan alpha) antibody stain. (**B**) DAPI nuclear counterstain of the field shown in **A**. (**C**) No primary antibody control. (**D**) DAPI counterstain of the field shown in **C**.

method. Specific immunofluorescence staining for Na_V (Pan α) was observed (Fig. 1), providing further evidence of sodium channel expression in the primary cultured osteoblasts.

The biophysical properties of endogenous inward sodium currents were analyzed in mouse primary calvarial osteoblasts using a high-throughput automated planar patch-clamp technology. Specifically, the voltage-dependence of activation, fast-inactivation, and recovery from fast inactivation were examined. Eight separate primary calvarial cell digests were utilized: data for CBZ are pooled from three digests and for PHT from a further two digests; the biophysical data are pooled from two digests. Representative current family traces illustrate the robust voltage-activated inward currents elicited in these cells (Fig. 2A). Current-voltage (I/V) curves, normalized to the maximum inward current were calculated, and as expected for Na_V, show a voltage dependence of activation, with the threshold of activation close to −40 mV and the peak current close to 0 mV (Fig. 2B). The voltage dependence of activation and fast-inactivation was examined by converting the peak current versus voltage curves into conductance versus voltage (G–V) and fit to a Boltzmann function (Fig. 2C). The half maximal voltage for activation and inactivation was -7.81 ± 0.47 mV and -42.9 ± 0.72 mV, respectively. The slope of the activation and inactivation curves was 7.71 ± 0.38 and 9.30 ± 0.63 (n = 13), respectively. Normalized current as a function of time following an inactivating voltage step was plotted, and the curve was fit with a hyperbola as a means to characterize data, for which the recovery constant was 1.59 ± 0.16 (n = 13) (Fig. 2D).

External application of CBZ resulted in significant inhibition of current amplitude, and this is reflected in the representative raw current traces obtained from a single cell using this voltage protocol (Fig. 3A). In the second set of experiments, cells were held at −60 mV, and on establishment of a stable baseline current, 50 μM CBZ was applied for 5 min (Fig. 3A). This revealed a block by CBZ and its subsequent wash-off, followed by almost complete block in the presence of TTX confirming presence of Na_V channels. The blocking effect of CBZ was consistent across all cells tested as highlighted by the averaged raw current traces (Fig. 3B) as well as the averaged and normalized I/V plots (Fig. 3C). CBZ caused a significant inhibition of current amplitude ($31.6 \pm 5.9\%$ inhibition, n = 9, $p < 0.001$) (Fig. 3D), which was partially reversed upon washout (see Fig. 3A inset), whereas its vehicle, DMSO, was without effect (data not shown). Furthermore, subsequent application of 10 μM TTX, a known sodium channel blocker, resulted in almost complete inhibition of the current ($89.96 \pm 2.14\%$ inhibition, n = 9, $p < 0.00001$) (Fig. 3D).

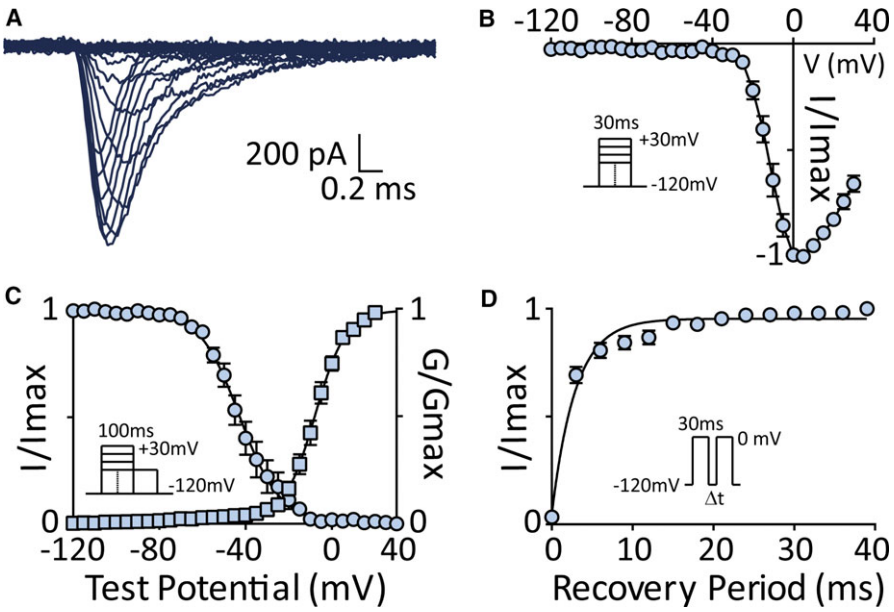

Figure 2.

Characterization of sodium currents recorded in mouse primary calvarial osteoblastic cells. (**A**) Representative current traces obtained from a single cell using a voltage dependence of activation protocol. (**B**) Normalized current-voltage relationship curve averaged from 13 cells. Inset shows the voltage protocol. (**C**) Voltage dependence of normalized peak conductance (□) and steady-state inactivation (○) shown as a function of voltage. Currents were normalized to the maximum peak current. Pulse protocol for steady-state inactivation shown in the inset. For both graphs, Boltzmann curves were fit to pooled averages (n = 13 cells) and plotted. (**D**) Recovery of channel availability from fast inactivation shown as a function of time. A hyperbola was fit to pooled averages and plotted. Schematic of pulse protocol is shown in the inset.

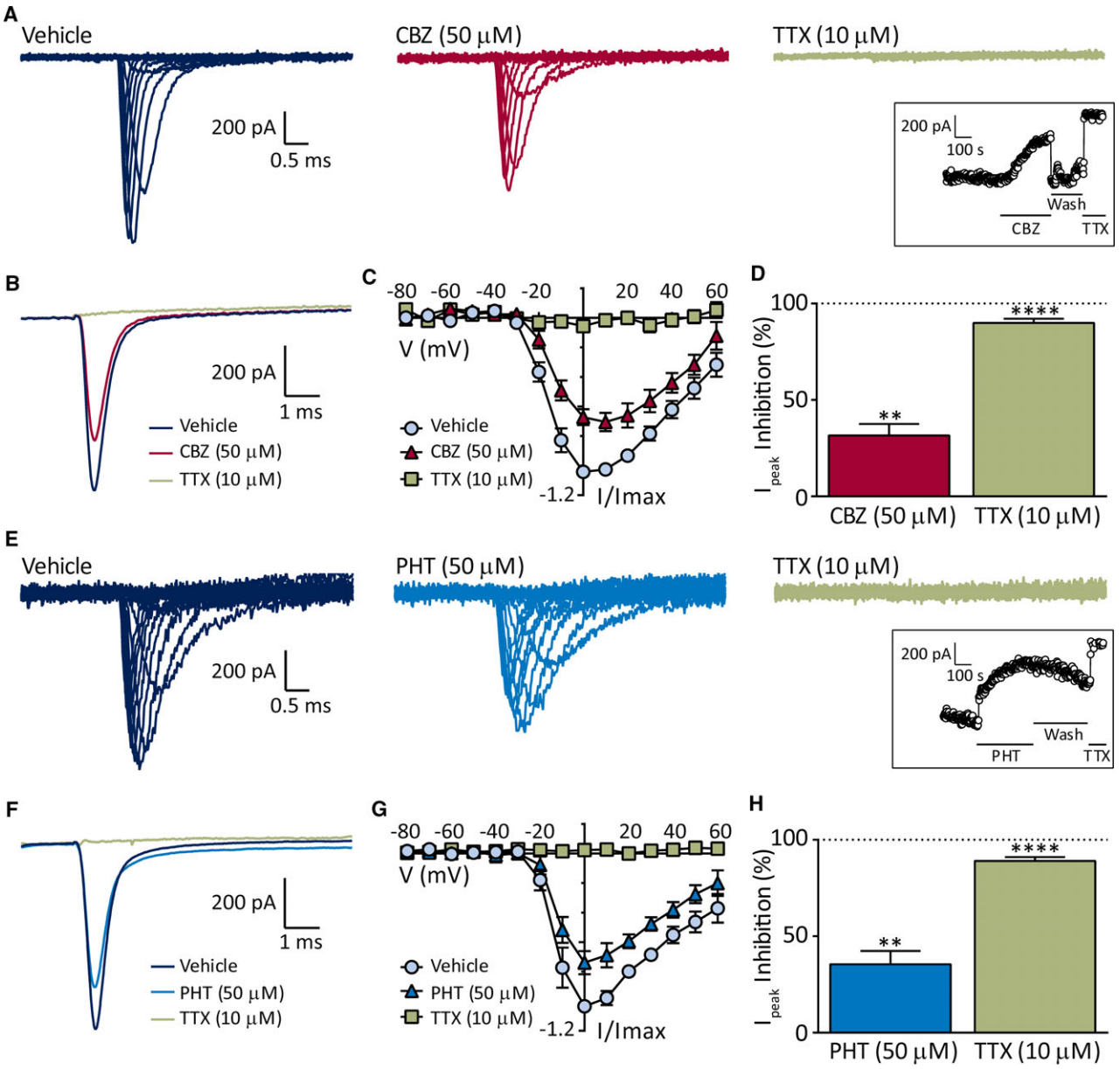

Figure 3.

Inhibitory effects of carbamazepine and phenytoin on voltage-dependent sodium currents recorded in C57BL/6J mouse primary calvarial osteoblasts. (**A**) INSET: Representative recording showing current traces obtained from a single cell in the presence of vehicle (navy traces), CBZ (50 μM; red traces) or TTX (10 μM; green traces), respectively. Cells were held at −60 mV and stepped from −80 mV to +60 mV for 20 msec every 2 s. Scale bars apply to all traces. Representative recording showing peak current plotted against time illustrating the blocking effect of CBZ, washout of CBZ, and subsequent block by TTX. (**B**) Averaged current traces in the presence of vehicle (navy trace), 50 μM CBZ (red trace), or 10 μM TTX (green trace). Cells were held at −60 mV and repeatedly stepped to 0 mV for 20 msec every 2 s (n = 9 cells). (**C**) Normalized average current-voltage relationships in the presence of vehicle (pale blue ○), 50 μM CBZ (red △), and 10 μM TTX (green □). Currents were normalized to the maximum peak current in the presence of vehicle (n = 9 cells). (**D**) Average percent inhibition by 50 μM CBZ (red) and 10 μM TTX (green) (n = 9 cells). (**E**) INSET: Representative recording showing peak current traces obtained from a single cell in the presence of vehicle (navy traces), PHT (50 μM; blue traces), or TTX (10 μM; green traces). Scale bars apply to all traces. Same voltage protocol as **A**. Representative recording showing peak current plotted against time illustrating the blocking effect of PHT, washout of PHT, and subsequent block by TTX. (**F**) Averaged current traces in the presence of vehicle (navy trace), 50 μM PHT (blue trace), or 10 μM TTX (green trace) (n = 7 cells). Same voltage protocol as **B**. (**G**) Normalized average current-voltage relationships in the presence of vehicle (pale blue ○), 50 μM PHT (blue △), and 10 μM TTX (green □). Currents were normalized to the peak current in the presence of vehicle (n = 7 cells). (**H**) Average percent inhibition by 50 μM PHT (blue) and 10 μM TTX (green) (n = 7 cells). For **D** and **H,** the peak currents in the presence of CBZ, PHT, or TTX were compared to the peak currents in the presence of vehicle. **$p < 0.01$, ****$p < 0.0001$.

In the next series of experiments, the effect of external application of PHT (50 μM) was examined. PHT also inhibited the TTX-sensitive current; however, this effect was not reversed upon washout (see Fig. 3E inset). Representative raw current traces from a single cell illustrate the degree of block by PHT and TTX (Fig. 3E). The averaged raw traces and the normalized I/Vs show the degree of block by PHT across several cells (Fig. 3F–G). The percent inhibition by PHT was statistically significant (35.5 ± 6.9% inhibition, n = 7, $p < 0.001$) (Fig. 3H).

Discussion

This study characterized the molecular and functional expression of Na_V channels in mouse primary calvarial osteoblasts and showed they were inhibited by the commonly prescribed AEDs CBZ and PHT. To our knowledge, this is the first study to report inhibitory effects of the AEDs CBZ and PHT on Na_V in osteoblastic cells, providing primary evidence for a direct effect on bone cells and, therefore, potentially on bone health. The electrophysiologic characteristics of the Na_V current in osteoblasts were found to be similar to those of neuronal sodium currents: the native osteoblastic sodium currents here were activated by depolarizations above −40 mV, exhibited steady-state fast inactivation with a V-half value around −43 mV, and were blocked by TTX.[32]

Although it has been demonstrated previously that osteoblasts are able to generate action potentials (APs),[20] the role and significance for these APs is not altogether clear. If APs were, for instance, generated during loading or stress detection, or initiate or contribute to signaling during bone remodeling, it is possible that AEDs that interfere with AP firing could increase fracture risk in patients medicated with certain AEDs. This effect could provide a mechanism by which a diverse group of molecules could have a similar, adverse effect on bone.

The genes identified in RNASeq analysis as being expressed by osteoblast cultures encode both the alpha pore forming and beta accessory subunits, indicating that functional Na_V channels are likely present in mouse osteoblasts. Both α and β subunits have important roles in the structure and function of Na_V: the α subunit forms the pore, whereas associated β subunits (which are also tissue specific), can direct trafficking and also modulate α-subunit function.[33,34] We note that cells utilized in the RNASeq were cultured utilizing media that was different from those utilized in immunocytochemistry and electrophysiologic experiments, and therefore it remains possible that other Na_V subtype expression under different media conditions, or at differing times in culture, are also present. Identifying functional expression of Na_V and investigating electrophysiologic responses of Na_V currents to AEDs was our primary aim, rather than specifically confirming the subtype acted upon by the AEDs examined in this study. The results of the RNASeq showed that of the genes encoding α subunits, the most highly expressed was *Scn7a* ($Na_Vi2.1$), which despite belonging to the family of Na_V channels, is a voltage- and TTX-insensitive sodium channel thought to be involved in sodium sensing and contributing to depolarization of the resting membrane potential in neurons.[35] As a channel that is thought to be Na^+ permeant at rest, it would exert a permanent depolarizing influence on the osteoblasts. The cellular role and effects of AEDs on $Na_Vi2.1$ are not known, partly due to the difficulty in obtaining functional heterologous expression.[36] Given that the currents recorded in this experiment were TTX sensitive (to TTX in the micromolar range), the recordings obtained here are not consistent with that of $Na_Vi2.1$ and are therefore more likely attributable to Na_V 1.2 and/or Na_V 1.3 TTX-sensitive currents.

A previous study showed that both PHT and CBZ inhibited proliferation of human osteoblast-like cells at therapeutic concentrations, indicating this decrease in proliferation may impair new bone formation.[7] However, electrophysiology was not performed to investigate specific effects at the ion channel level. Altered membrane potential and reduced electrical coupling via gap junctions in the presence of CBZ and PHT[37] have been shown in a previous study of rat primary osteoblasts; however, Na_V channels were not examined. Further studies are required to examine the effects of other AEDs on Na_V channels as well as other ion channels in osteoblasts, osteocytes, osteoclasts, and in human cells to further explore the effects of AEDs on bone health.

These in vitro studies have demonstrated osteoblast ion channels that are sensitive to inhibition by two common AEDs, providing a potential mechanism of increased fracture risk in patients via direct effects of AEDs on osteoblast function.

Acknowledgments and Funding

The authors would like to sincerely acknowledge the following organizations for funding received during the development of this study including: the Molly McDonnell Foundation Scholarship (2009), DW Keir Fellowship in Medical Research at The Royal Melbourne Hospital (January 2010–June 2012), University of Melbourne Early Career Researcher (ECR) grant (2010), Brain Foundation Research Grant-in-Aid (2011), The Royal Melbourne Hospital Home Lottery Grants-in-Aid (2012), RACP Servier Barry Young Fellowship in Neuroscience (2012), The Royal Melbourne Hospital Victor Hurley Grants-in-Aid (2013), MBC Postdoctoral Medical Research Fellowship at The Melbourne Brain Centre RMH (June 2012–2014), and (NHMRC Centre for Research Excellence Grant 1001216). Dr. Sandra Petty held the Thwaites Gutch Fellowship at Ormond College Parkville 2011–2015.

Disclosure

None of the authors has any conflict of interest to disclose. We confirm that we have read the Journal's position on issues involved in ethical publication and affirm that this report is consistent with those guidelines.

References

1. Vestergaard P. Epilepsy, osteoporosis and fracture risk – a meta-analysis. *Acta Neurol Scand* 2005;112:277–286.
2. Petty SJ, Paton LM, O'Brien TJ, et al. Effect of antiepileptic medication on bone mineral measures. *Neurology* 2005;65:1358–1365.
3. Andress DL, Ozuna J, Tirschwell D, et al. Antiepileptic drug-induced bone loss in young male patients who have seizures. *Arch Neurol* 2002;59:781–786.
4. Moro-Alvarez MJ, Diaz Curiel M, de la Piedra C, et al. Bone disease induced by phenytoin therapy: clinical and experimental study. *Eur Neurol* 2009;62:219–230.
5. Petty SJ, O'Brien TJ, Wark JD. Anti-epileptic medication and bone health. *Osteoporos Int* 2007;18:129–142.
6. Sander JW. The epidemiology of epilepsy revisited. *Curr Opin Neurol* 2003;16:165–170.
7. Feldkamp J, Becker A, Witte OW, et al. Long-term anticonvulsant therapy leads to low bone mineral density–evidence for direct drug effects of phenytoin and carbamazepine on human osteoblast-like cells. *Exp Clin Endocrinol Diabetes* 2000;108:37–43.
8. Cummings SR, Nevitt MC, Browner WS, et al. Risk factors for hip fracture in white women. Study of Osteoporotic Fractures Research Group. *N Engl J Med* 1995;332:767–773.
9. Fitzpatrick LA. Pathophysiology of bone loss in patients receiving anticonvulsant therapy. *Epilepsy Behav* 2004;5(Suppl. 2):S3–S15.
10. Sato Y, Kondo I, Ishida S, et al. Decreased bone mass and increased bone turnover with valproate therapy in adults with epilepsy. *Neurology* 2001;57:445–449.
11. Ensrud KE, Walczak TS, Blackwell TL, et al. Antiepileptic drug use and rates of hip bone loss in older men: a prospective study. *Neurology* 2008;71:723–730.
12. Rawlinson SC, Pitsillides AA, Lanyon LE. Involvement of different ion channels in osteoblasts' and osteocytes' early responses to mechanical strain. *Bone* 1996;19:609–614.
13. Zanello LP, Norman AW. Multiple molecular mechanisms of 1 alpha,25(OH)2-vitamin D3 rapid modulation of three ion channel activities in osteoblasts. *Bone* 2003;33:71–79.
14. Black JA, Waxman SG. Sodium channel expression: a dynamic process in neurons and non-neuronal cells. *Dev Neurosci* 1996;18: 139–152.
15. Chakkalakal DA. Mechanoelectric transduction in bone. *J Mater Res* 1989;4:1034–1046.
16. Pavalko FM, Norvell SM, Burr DB, et al. A model for mechanotransduction in bone cells: the load-bearing mechanosomes. *J Cell Biochem* 2003;88:104–112.
17. Turner CH, Pavalko FM. Mechanotransduction and functional response of the skeleton to physical stress: the mechanisms and mechanics of bone adaptation. *J Orthop Sci* 1998;3:346–355.
18. Sun J, Liu X, Tong J, et al. Fluid shear stress induces calcium transients in osteoblasts through depolarization of osteoblastic membrane. *J Biomech* 2014;47:3903–3908.
19. Chesnoy-Marchais D, Fritsch J. Activation of hyperpolarization and atypical osmosensitivity of a Cl- current in rat osteoblastic cells. *J Membr Biol* 1994;140:173–188.
20. Pangalos M, Bintig W, Schlingmann B, et al. Action potentials in primary osteoblasts and in the MG-63 osteoblast-like cell line. *J Bioenerg Biomembr* 2011;43:311–322.
21. Zanello LP, Norman A. 1alpha,25(OH)2 vitamin D3 actions on ion channels in osteoblasts. *Steroids* 2006;71:291–297.
22. Hodgkin AL, Huxley AF. A quantitative description of membrane current and its application to conduction and excitation in nerve. *J Physiol* 1952;117:500–544.
23. Black JA, Waxman SG. Noncanonical roles of voltage-gated sodium channels. *Neuron* 2013;80:280–291.
24. Vestergaard P, Rejnmark L, Mosekilde L. Fracture risk associated with use of antiepileptic drugs. *Epilepsia* 2004;45:1330–1337.
25. Lee RH, Lyles KW, Colon-Emeric C. A review of the effect of anticonvulsant medications on bone mineral density and fracture risk. *Am J Geriatr Pharmacother* 2010;8:34–46.
26. Pack AM. Treatment of epilepsy to optimize bone health. *Curr Treat Options Neurol* 2011;13:346–354.
27. Pagel CN, Song SJ, Loh LH, et al. Thrombin-stimulated growth factor and cytokine expression in osteoblasts is mediated by protease-activated receptor-1 and prostanoids. *Bone* 2009;44:813–821.
28. National Health and Medical Research Council. *Australian Code for the Care and Use of Animals for Scientific Purposes*, 8th ed. Canberra: National Health and Medical Research Council, 2013.
29. Trapnell C, Salzberg SL. How to map billions of short reads onto genomes. *Nat Biotechnol* 2009;27:455–457.
30. Trapnell C, Williams BA, Pertea G, et al. Transcript assembly and quantification by RNA-Seq reveals unannotated transcripts and isoform switching during cell differentiation. *Nat Biotechnol* 2010; 28:511–515.
31. Ramskold D, Wang ET, Burge CB, et al. An abundance of ubiquitously expressed genes revealed by tissue transcriptome sequence data. *PLoS Comput Biol* 2009;5:e1000598.
32. Waxman SG. Sodium channels, the electrogenisome and the electrogenistat: lessons and questions from the clinic. *J Physiol* 2012;590:2601–2612.
33. Patino GA, Isom LL. Electrophysiology and beyond: multiple roles of Na+ channel beta subunits in development and disease. *Neurosci Lett* 2010;486:53–59.
34. Namadurai S, Yereddi NR, Cusdin FS, et al. A new look at sodium channel beta subunits. *Open Biol* 2015;5:140192.
35. Ke CB, He WS, Li CJ, et al. Enhanced SCN7A/Nax expression contributes to bone cancer pain by increasing excitability of neurons in dorsal root ganglion. *Neuroscience* 2012;227:80–89.
36. Savio-Galimberti E, Gollob MH, Darbar D. Voltage-gated sodium channels: biophysics, pharmacology, and related channelopathies. *Front Pharmacol* 2012;3:124.
37. Schirrmacher K, Brummer F, Dusing R, et al. Dye and electric coupling between osteoblast-like cells in culture. *Calcif Tissue Int* 1993;53:53–60.